Astron. Astrophys. 250, 475–483 (1991)

ASTRONOMY AND ASTROPHYSICS

Radiatively and shock excited H_2 in Magellanic H II regions*

F.P. Israel[1] **and J. Koorneef**[2,**]

[1] Sterrewacht Leiden, Postbus 9513, NL-2300 RA Leiden, The Netherlands
[2] Space Telescope Science Institute, Homewood Campus, Johns Hopkins University, Baltimore, MD 21218, USA

Received January 2, accepted March 15, 1991

Abstract. Near-IR spectroscopy of 14 small Magellanic Cloud H II regions has led to the detection of the 1–0 S (1) transition of molecular hydrogen (H_2) in 8 objects. In the latter, relatively strong emission due to the He I 4^3S–3^3P^0 transition was also found. As a consequence, low-resolution CVF spectrophotometry of (extragalactic) H II regions carries the danger of significantly overestimating the 1–0 S (1) H_2 transition strength, and thereby the relative importance of shock excitation.

In 5 objects (SMC: N81, N88; LMC: N83B, N159A5 and N160A2) various H_2 transitions were observed in order to identify the H_2 excitation mechanism. Observed line ratios indicate that N83B and N81 are radiatively excited. The remaining objects either contain a shock-excited H_2 component or have densities sufficiently high that collisional de-excitation influences observed line ratios. However, in both cases radiative excitation is in all objects the energetically dominant mechanism. For the observed H_2 Clouds, we derive volume densities n_H = 2000–10 000 cm^{-3}, with a mean of 5000 cm^{-3}. If significant subparsec clumping occurs, densities may be higher. Limits on shock contributions to the observed H_2 emission suggest shock velocities $V_s < 10\ km\,s^{-1}$ (J-type shocks) or $V_s < 15$–$23\ km\,s^{-1}$ (C-type shocks). In turn, this suggests that early-type stars in the observed objects have stellar winds weaker than Galactic O-type stars.

The strength of the observed near-IR He I transitions is briefly discussed. Further investigation of He I lines in Magellanic Cloud H II regions may be of interest.

Key words: Galaxies: Magellanic Clouds – H_2 clouds: excitation – density – stellar mass loss – H II regions: molecular clouds – helium line strengths

1. Introduction

Cold molecular hydrogen, although a major constituent of the interstellar medium, is hard to observe directly. When excited by shocks or ultraviolet radiation fields, however, it is observable by its rotation–vibration transitions in the near-IR . In the Milky Way, a variety of objects has thus been found to be associated with molecular hydrogen. The detected emission is in most cases due to shocked molecular gas. To a certain extent, this may be the consequence of selection effects: small observing apertures, and small beam-chops emphasize high-surface-brightness structures of limited extent, at the cost of more extended emission of lower surface brightness.

In previous papers (Koornneef & Israel 1985, hereafter Paper I; Israel & Koornneef 1988 Paper II) we have reported the detection of molecular hydrogen emission towards H II regions in the Magellanic Clouds. Most of those observations were obtained with circular variable filterwheel (CVF) detectors of limited spectral resolution (typically $\lambda/\Delta\lambda = 100$). Such a resolution is generally insufficient to clearly separate line emission from the underlying continuum. As a consequence, line ratios useful as diagnostics for the excitation mechanism (shock or radiative) are hard to determine. Yet, knowledge of the excitation mechanism is essential for the proper interpretation of the observations. For this reason, we have observed over a dozen Magellanic Cloud H II regions with the higher spectral resolution supplied by a cooled grating spectrometer.

2. Observations

The data presented here were obtained in two observing runs (January 1988 and November 1988). On both occasions we used the infrared grating spectrometer (IRSPEC, cf. Moorwood et al. 1986) on the 3.6 m telescope at the European Southern Observatory. The spectrograph uses a 32 element array with a pixel spacing of $\lambda/\Delta\lambda$ 1600 at 2.2 μm. The actual resolution of the spectrograph is better than that, so that lines narrower than a few hundred $km\,s^{-1}$ are undersampled. We found the sensitivity of the instrument to be very stable within a single observing period, but measured variations of several tens of per cent from run-to-run. Typically, narrow emission features with a line flux of $1.0\ 10^{-21}\ W\,cm^{-2}$ can be measured with an accuracy of about 20% in an hour of elapsed observing time. All observations were chopped in a north–south direction with chops of 20 to 30 arcsec. Data analysis showed that significant spectral structure can occur in the "zero-flux" baselines even for observations in spectral regions generally considered "clear", such as the H and K atmospheric windows. As the penalty in observing time is minimal, we included beam-switching in addition to chopping in our routine observing strategy.

Wavelength calibration was done by obtaining spectra of a built-in neon lamp. For flux calibration we used the standard

Send offprint requests to: F.P. Israel

* Based on observations collected at the European Southern Observatory (ESO) at La Silla, Chile

** On assignment from the Astrophysics Division, Space Science Department, European Space Agency (ESA) stars HR 191, HR 2290, HR 4523 and HR 6072 (Koornneef 1983a, b). We did not observe all standards at all grating settings, but found that HR 191 has significant hydrogen absorption H 11–4 at 1.681 μm for which we corrected; we also see some H 7–4 absorption at 2.166 μm in HR 2290. Otherwise, the flux distributions of our calibrators appear well represented by simple polynomials.

To convert flux to surface brightness we use the nominal physical size of the entrance aperture (6 × 6 arcsec, or 0.846 nsr). As the instrumental response to a point source is quite sensitive to the position within the aperture even during periods of excellent seeing, this conversion will lead to an underestimate of the surface brightness for those sources that fill the aperture in a more uniform manner.

Data analysis is relatively straightforward. The first step is to discard data affected by cosmic ray hits (spikes). On science targets, we collected chopped observations on a single position for about 15 min. For such a data set, we separated the read-outs of the two chopper positions and removed those data points that were statistically out of range. While only a third to half of the (15 min) spectra have one or more cosmic ray hits, their effect on the spectra is quite disastrous as their appearance closely mimics that of unresolved emission lines. We consider their removal essential for reliable work at the intensity levels considered here. After despiking, positive and negative beams are combined in the usual manner. We then applied a (spectral) vignetting function to compensate for some instrumental curvature of the spectrum. The apparent light loss is 10–20% at the extreme ends of each spectrum and follows directly from the observations of the calibration standard stars. The actual vignetting is much less for spatially extended sources, which therefore tend to be overcorrected. Extinction coefficients and count-to-flux conversions are then applied to each individual pixel. We did not independently determine the grey component of the atmospheric extinction but instead adopted typical values from infrared filter photometry. Extinction was assumed to depend linearly on air mass which is adequate for the limited air mass range of our data set, except for some very narrow and deep absorption lines at 2.418 μm which left significant residuals. We also found indications that these atmospheric lines vary in strength even during stable weather, presumably due to changes in the precipitable water vapour content of the higher atmosphere.

Repeated read-outs within one data set allow derivation of an internal error for each particular pointing. We carry this error through the process of beam-combining, devignetting, atmospheric correction and flux calibration, and display the resulting information on each of the individual plots (Fig. 1). We also use the error bars as weighting functions in fitting continuum and line profiles. Systematic errors, most of the sources of which have been introduced above, will be discussed in the tesxt where appropriate. All fluxes and errors quoted in this paper have been determined by a fitting routine operating on the whole observed spectrum.

3. Results and analysis

3.1. Nature of sample

In Table 1, we summarize the observational results obtained at the wavelength of the 1–0 S(1) transition of H_2 (2.121 μm). Column 2 gives the (generally weak) continuum, while column 3 gives the observed 1–0 S(1) line strength. All sources detected previously in the 1–0 Q-branch (SMC: N81, N88; LMC: N11A, N83B, N159A5) are now confirmed, even when before no 1–0 S(1) line was detected with the CVF. In addition, we detected H_2 emission from N150, N160A1 and N160A2. All clearly detected objects belong to *the same class* of highly excited small H II regions that was found optically in the Magellanic Clouds (Testor & Pakull 1985; Heydari-Malayeri & Testor 1985, 1986; Heydari-Malayeri et al. 1988; Heydari-Malayeri et al. 1990). These objects are characterized by compactness, high density and high excitation. Only the nature of N150 is presently unknown; it was selected for observation because of its compactness and very red colours in unpublished near-IR photometry, which suggests that it is an embedded young object of the same type as the others.

Marginally or not detected are N84B3 and N66 in the SMC, and N55, N213A, N214AB and N159S in the LMC. Both N55 and N66 are extended objects; we sampled only a single position (IRAS 12 μm peak). The SMC-nebula N84B3 (Testor & Lortet 1987) was observed because of its large L' excess in $JHKL'$ photometry. The present result suggests that the near-IR emission is largely due to a dust shell around an evolved star. The same conclusion applies to LMC-N214AB. N213A is probably an evolved nebula; Brackett-γ emission was detected (Paper II), but no H_2 has been found. Finally, $JHKL'$ photometry of N159S shows it to be as red as N159A5, a true compact nebula. However, analysis of the N159S near-IR continuum, as well as its lack of H_2 suggests it is also an evolved star with a dust shell. This result emphasizes the difficulty in differentiating between old and young dust-embedded objects from photometry alone.

The spectral fitting procedure yielded estimates of the level of continuum emission with a typical internal accuracy of 10^{-19} W cm^{-2} μm^{-1}, corresponding to 0.3 λ^2 mJy. These values can be compared to those obtained from broadband K photometry. Comparison (Table 1) shows that the two determinations are in excellent agreement. This has two implications: (a) the continuum levels obtained from beam-switched/chopped spectrophotometry are reliable; (b) because the broadband photometry was obtained with a larger aperture of 10 arcsec, the continuum sources must have typical sizes not larger than the IRSPEC aperture of 6 arcsec (about 1.7 pc).

Table 1 contains two entries for N81 and N160A2. These refer to the observations made in January 1988 (top line) and November 1988 (bottom line), respectively. The difference in results indicates that in spite of our efforts, the pointing in the two runs must have been slightly different.

3.2. Extent of emission in N88

We have mapped the extent of emission associated with N88 in both the east–west and north–south direction (Fig. 3). In the east–west direction, comparison with the profile of the standard star HR 191 shows that both the 1–0 S(1) and He I (4^3 S–3^3 P^0) emission are unresolved (deconvolved diameter less than 0.9 pc), whereas the continuum has a (deconvolved) half-width diameter of 1.2 pc. In the north–south direction, the continuum, as well as the 1–0 S(1) and He I emission are resolved, with (deconvolved) diameters of 1.8, 1.6 and 2.2 pc. Although the H_2 and He I clouds are of very similar extent, the He I peak appears displaced from the 1–0 S(1) H_2 peak by about 0.5 pc in a southeastern direction. Its position agrees, to within the errors of observation, with the continuum peak position; consequently, the H_2 peak is also

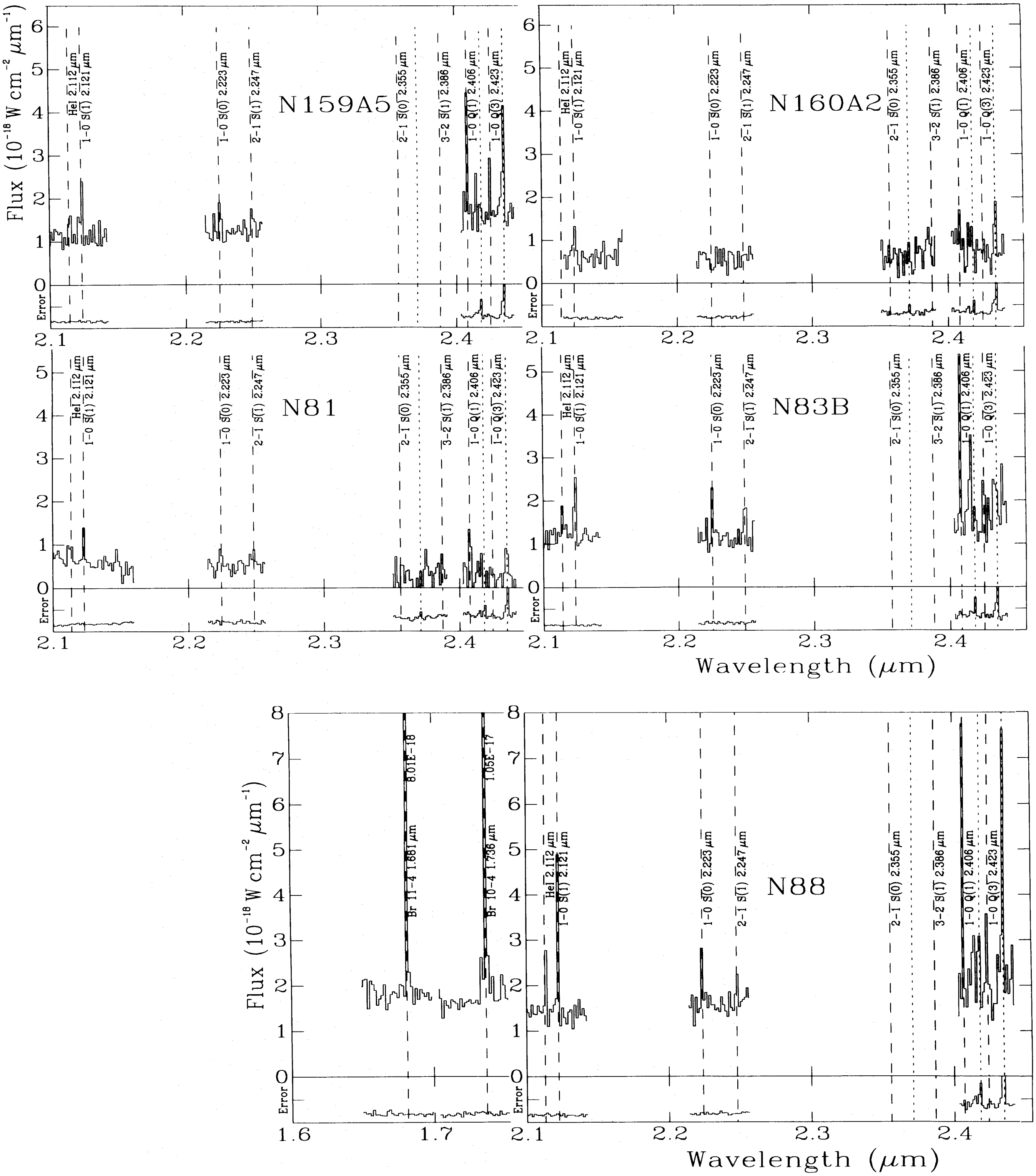

Fig. 1. Combined spectra of SMC N81, N88, LMC N83B, N159A5 and N160A2, corresponding to the data in Table 2. Data summarized in Table 1 and not shown here are of similar quality. Formal 1σ errors are shown as a function of wavelength (cf. Sect. 2). Large errors longwards of 2.4 μm are due to strong atmospheric absorption features (dotted lines). H, He I and H_2 transitions (dashed lines) have been identified. The 1–0 Q(2) line at 2.413 μm is clearly present in the spectra but has not been marked for lack of space. The 1–0 Q(4) line at 2.437 μm may be present in the N83B spectrum

displaced from the continuum peak. The data in Table 1 suggest that the two peaks likewise do not coincide in LMC-N160A2 but probably do coincide in SMC-N81.

The extent of excited H_2 in N88 is rather similar to the size of the H II region, and much smaller than the 6 pc diameter of the associated CO cloud (unpublished observations). Thus, as is to be

Table 1. Magellanic Clouds 1–0 S(1) measurements[a]

Object		Continuum[b] 10^{-17} ($W\,cm^{-2}\,\mu m^{-1}$)	1–0 S(1) 2.121 μm (10^{-21} $W\,cm^{-2}$)	He I 4^3S–3^3P^0 2.112 μm (10^{-21} $W\,cm^{-2}$)	4^1S–3^1P^0 2.114 μm (10^{-21} $W\,cm^{-2}$)
SMC	N66	0.02 (—)	0.7 ± 0.6	<0.6	<0.7
	N81	0.07 (0.08)	1.9 ± 0.4	0.5 ± 0.3	<0.4
		0.05[c]	1.4 ± 0.2	—	—
	N84B3	0 (0.01)	0.75 ± 0.65	<0.85	1.0 ± 0.75
	N88	0.13 (0.15)	6.0 ± 0.3	2.4 ± 0.4	<0.3
LMC	N11A	0.05 (0.07)	1.8 ± 0.4	0.7 ± 0.55	0.45 ± 0.35
	N55	0.03 (—)	0.85 ± 0.5	—	—
	N83B	0.11 (0.10)	3.1 ± 0.3	1.3 ± 0.25	0.5 ± 0.25
	N150	0.04 (0.04)	1.5 ± 0.4	0.85 ± 0.6	<0.3
	N213A	0.03 (0.03)	<0.55	<0.5	<0.5
	N214AB	0.04 (0.03)	0.5 ± 0.4	<0.6	<0.4
	N159A5	0.11 (0.11)	2.3 ± 0.3	1.2 ± 0.35	<0.3
	N159S	0.08 (0.10)	0.55 ± 0.35	<0.3	<0.3
	N160A1	0.12 (—)	0.9 ± 0.3	1.4 ± 0.25	0.6 ± 0.3
	N160A2	0.22 (—)	1.0 ± 0.2	2.7 ± 0.3	0.8 ± 0.4
		0.05[c]	1.7 ± 0.5	—	—

Notes

[a] Unless otherwise stated January 1988 observations

[b] Uncertainty in continuum <0.01 10^{-17} $W\,cm^{-2}\,\mu m^{-1}$; values in parentheses are broadband K photometric values

[c] November 1988 observations

expected, the observed H_2 cloud appears to represent the *warm interface* of the small H II region with its larger associated cold molecular cloud.

3.3. H_2 line ratios and excitation

Towards five of the brightest regions, N81, N88 (SMC) and N83B, N159A5, N160A2 (LMC), we have attempted to measure other H_2 transitions, so as to derive line ratios that are useful in determining the excitation mechanism. The observed line strengths are given in Table 2; Table 3 lists the most important strengths with respect to the 1–0 S(1) line. In Table 3 we also give model strengths for different physical conditions. The important 2–1 S(1) and 1–0 S(0) lines were detected in all sources, except N160A2. Also, in all sources except N160A2 the 1–0 Q(1) line was detected with considerable strength. The other Q-branch transition intensities are somewhat less reliable, because of increasing atmospheric problems. By assuming an unreddened value of 0.70, we have derived nominal extinctions at the wavelength of the 1–0 S(1) line from the observed (1–0 Q(3)/1–0 S(1)) line ratio. N83B and N159A5 appear to suffer a certain amount of extinction, but the results given in Table 4 suffer from relatively large errors. For comparison we have also listed nebular extinctions, determined from the Balmer decrement. Although these are underestimates, they indicate relatively small extinctions of the order of 0.1–0.2 mag at near-IR wavelengths. A notable exception is N83B, where the (2–1 S(1)/1–0 S(1)) ratio indicates a rather high 2.1 μ extinction (cf. Fig. 4 below), comparable to the uncertain value derived from the nominal (1–0 Q(3)/1–0 S(1)) ratio.

Model and observed (2–1 S(1)/1–0 S(1)) and (1–0 S(0)/1–0 S(1)) ratios are graphically shown in Fig. 4. The model shock ratios were taken from Black & van Dishoeck (1987) (hereafter BvD). They apply to thermal gas radiating in LTE at $T = 1000$ K and 2000 K, respectively. Strictly, speaking, this supposes gas densities of the order of $3\,10^5$ cm^{-3}. At lower densities, predicted shock line ratios are slightly different (see Shull & Hollenbach 1978), but this does not influence the interpretation of our results. The model radiative excitation ratios were supplied by van Dishoeck & Black (private communication) and apply to LMC metallicities, $n_H = 1000$ cm^{-3}, $I_{UV} = 100$ and $T = 100$ K and 50 K, respectively. Here and in the following, I_{UV} is the strength of the ambient UV radiation field with respect to that in the Solar Neighbourhood ($I_{1000\,Å} = 4.5\,10^{-8}$ photons $s^{-1}\,cm^{-2}\,Hz^{-1}$; BvD). For comparison, we also include the M33-NGC604 measurements (Israel et al. 1989). The calculations by BvD for Galactic metallicities show that at constant temperature T the model ratios for $I_{UV} = 10^4$–10^5 (as found for the sources observed by us) differ little from those for $I_{UV} = 100$.

Figure 3 shows that, as is the case for M33-NGC604, the H_2 line ratios in LMC-N83B and SMC-N81 (two determinations) are explained satisfactorily by pure radiative fluorescent emission. The line ratios of the other objects (including N160A2) can be explained by assuming a mixture of radiative fluorescent and shock emission, as in Orion (see below). In addition, it appears that the radiatively excited component in LMC-N159A5 is relatively cool ($T = 50$ K), whereas the other sources can all be fitted with a hotter (100 K) radiatively excited component. A more quantitative analysis then suggests that the 1–0 S(1)

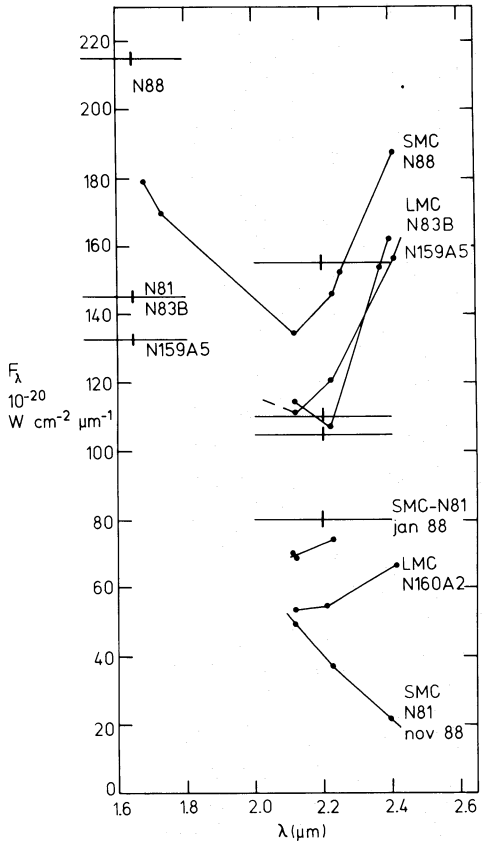

Fig. 2. Continuum strength throughout the K-band window (froor N88 also H-band window) as determined from IRSPEC observations. Broad-band photometry fluxes are marked by large crosses. Note spectral upturn around 2.1 µm, where dominant stellar emission is replaced by nebular and especially hot-dust emission. The November 1988 continuum of N81 is apparently stellar up to 2.4 µm

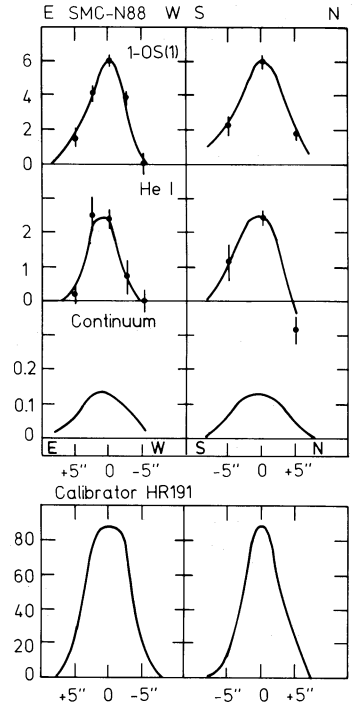

Fig. 3. Distribution of 1–0 S(1), He I and continuum emission through N88 in EW and NS directions. For comparison, the EW and NS (beam) profiles through the calibrator star HR 191 are also shown

emission from N88 is 70±5% shock-excited, while for N159A5 and N160A2 the corresponding values are 60±15% and >60%, respectively.

As an alternative we should consider that in SMC-N88, LMC-159A5 and N160A2 the undoubtedly present strong UV radiation fields might conspire with high local densities $n(H_2) > 10^4\ cm^{-3}$ to produce collisionally de-excited emission with lower v-level line ratios mimicking those of shock-excited emission (cf. Sternberg & Dalgarno 1989). The ratios in Table 3 indicate that if this process occurs, only a small contribution is sufficient to reduce a possible shock-excited contribution to zero. At present, we cannot rule out this possibility.

3.4. *Physical condition of radiatively excited H_2*

For a further analysis, we first estimate the strength of the ultraviolet radiation field at the cloud edge, assuming the H_2 cloud to border on the H II region (cf. Sect. 3.2). The H II region sizes, and the luminosity of the exciting stars were taken from the published literature, assuming standard OB-star parameters as given by Panagia (1973). Following a procedure similar to that used by Israel et al. (1989) we find that exciting stars with a luminosity of $10^6 L_\odot$ create a photon flux of $5\ 10^{-4} d^{-2}$ photons $s^{-1}\ cm^{-2}\ Hz^{-1}$ at a distance of d pc to the stars. The observed luminosities and H II region radii and the resulting values for I_{UV} are given in Table 4. We also list the surface brightness σ(S1) of the 1–0 S(1) line, as well as the surface brightness of the shocked and radiatively excited 1–0 S(1) emission components based on the decomposition illustrated in Fig. 3. From these, the total H_2 surface brightness $\sigma(H_2)$ is derived. Model calculations (BvD; van Dishoeck & Black, private communication) show that the ratio $\sigma(H_2)/\sigma(S1)$ is about 60, 75 and 10, respectively for LMC radiative excitation at $T = 100$ K, $T = 50$ K and shock excitation. This leads to the values given in Table 4, which clearly show that the total H_2 emission is *dominated* completely by radiatively excited emission. If the previously mentioned collisional de-excitation occurs, inferred shock contributions are even less. The shock values in Table 4 should then be read as upper limits.

This is the same result found for the Orion H_2 cloud, where radiatively excited emission is about three times more luminous than shock-excited H_2 emission, notwithstanding the locally much higher surface brightness of the latter (Burton & Puxley 1990). The total H_2 luminosity of Orion, corrected for extinction is of the order of $L(H_2) = 385\ L_\odot$ (ibidem); for the Magellanic Cloud sources we find H_2 luminosities ranging from 65 to 200 $L_\odot$, not corrected for extinction, nor for extent beyond the roughly 2 pc aperture. If no shock contribution is present at all, the H_2 luminosity of our sources will range from 120 to 600 $L_\odot$. Thus, the Magellanic Cloud sources detected by us are very *similar* to the Galactic Orion H_2 cloud with regard to both *luminosity and excitation.*

For radiatively excited H_2, the surface brightness scales with total hydrogen density $n_H = n(HI) + 2N(H_2)$. The models by van Dishoeck & Black (private communication) and the values listed

Table 2. Magellanic Clouds H_2 transitions[a]

Transition	SMC N81[b] (10^{-21} W cm^{-2} μm^{-1})	LMC N88 (10^{-21} W cm^{-2} μm^{-1})	LMC N83B (10^{-21} W cm^{-2} μm^{-1})	LMC N159A5 (10^{-21} W cm^{-2} μm^{-1})	LMC N160A2[b] (10^{-21} W cm^{-2} μm^{-1})
1–0 S(0)	0.8±0.3	2.2±0.3	2.0±0.4	1.4±0.3	<0.5
2–1 S(0)	<0.6	—	—	—	<0.5
1–0 S(1)	1.4±0.3	6.0±0.3	3.1±0.3	2.3±0.3	1.7±0.5
2–1 S(1)	0.6±0.3	1.2±0.2	1.9±0.3	0.5±0.3	<0.5
3–2 S(1)	0.8±0.8	—	—	—	<0.8
2–1 S(2)	<0.3	—	—	—	<0.5
1–0 Q(1)	2.3±0.8	9.8±0.8	6.7±0.7	5.0±0.3	1.3±0.6
1–0 Q(2)	—	3.0±0.9	4.3±0.8	1.5±0.5	1.0±0.8
1–0 Q(3)	<2.0	4.3±1.0	2.9±1.2	2.2±0.5	<0.7
1–0 Q(4)	—	<0.7	2.1±0.6	<0.4	<0.8
7–5 Q(1)	—	<0.4	—	—	—
6–4 O2	—	<0.4	—	—	—
6–4 O3	—	1.2±0.6	—	—	—
5–3 O4	—	<0.4	—	—	—
H 10–4	—	15.7±0.4	—	—	—
H 11–4	—	11.1±0.4	—	—	—
H 20–5	<0.8	1.4±0.7	1.7±0.9	0.8±0.4:	<1.1
H 22–5[c]	—	<0.3	<0.8	0.4±0.3	—

Notes
[a] Unless otherwise stated January 1988 observations
[b] November 1988 observations
[c] H 21–5 obliterated by atmospheric absorption

Table 3. Magellanic Clouds H_2 transition ratios

Transition	SMC N81	LMC N88	LMC N83B	LMC N159A5	LMC N160A2
1–0 S(0)	0.57±0.23	0.37±0.05	0.65±0.13	0.61±0.15	<0.35
2–1 S(0)	<0.43	—	—	—	—
1–0 S(1)	1.00	1.00	1.00	1.00	1.00
2–1 S(1)	0.43±0.23	0.20±0.04	0.61±0.10	0.26±0.13	<0.47
3–2 S(1)	0.57±0.57	—	—	—	—
2–1 S(2)	<0.16	—	—	—	—
1–0 Q(1)	1.71±0.52	1.63±0.13	2.16±0.30	2.17±0.40	0.76±0.35
1–0 Q(2)	—	0.50±0.15	1.39±0.26	0.65±0.22	0.59±0.47
1–0 Q(3)	<1.4	0.72±0.17	0.95±0.40	0.96±0.22	—
1–0 Q(4)	—	<0.12	0.68±0.19	<0.17	—
6–4 O2	—	0.12±0.06	—	—	—
6–4 O3	—	0.20±0.10	—	—	—
5–3 O4	—	<0.07	—	—	—

in Table 4 yield mean densities $n_{\rm H}=2\,10^3$–$1\,10^4$ cm^{-3}, with a mean around $5\,10^3$ cm^{-3}. The results from Paper II and our mapping of N88 indicate that the H_2 emitting regions are of sizes equal to or larger than the observing aperture. The aperture size corresponds to about 1.6 pc at the distance of the clouds. Thus, aperture-filling factors should be of order unity unless significant structure on subparsec scales is present. A more quantitative estimate can be made for N88. The value in Table 4, $n_{\rm H}=$ 5000 cm^{-3}, can be compared to the highest densities of the H II region ($n_e=1600$ cm^{-3}; Testor & Pakull 1985). As the H_2 emitting region has a size comparable to that of our aperture, we can derive an estimate for the H_2 filling factor. If the cloud were a homogeneous sphere with a diameter of 1.25 pc, its mass would be of the order of 270 $M_\odot$. However, Testor & Pakull (1985) find a H II mass for N88 of 20–50 $M_\odot$. Also, from unpublished CO observations we derive a total mass for the molecular cloud, to which N88 belongs, of the order of 4000 $M_\odot$. This cloud has about hundred times the volume (25 times the surface area) of N88. A (surface) filling factor of 0.3 therefore seems reasonable. If the H_2 gas were in a shell with roughly spherical symmetry, it would then have a thickness of 0.15 pc at a radius of 0.75 pc.

This would raise the H_2 surface brightness and thus the hydrogen density by a factor of three. Even then, the pressure of the H II region exceeds that of the H_2 zone by roughly an order of

Table 4. Properties of detected H_2 clouds

	SMC N81	LMC N88	N83B	N159A5	N160A2
A_{21}[a] (mag)	<1.4	<1.3	1.8±1.8	1.7±1.2	—
A_V (H II)[b] (mag)	0.2	1.7	3.7	2.3	0.8
Diameter[b] (pc)	1.95	0.75	0.6	1.45	1.75
L_*[b] ($10^6\ L_\odot$)	0.6	1	0.5	1.3	0.5
I_{UV}[c]	7000	81 000	60 000	28 000	7000
H_2 Aperture-averaged line surface brightness (10^{-5} erg s^{-1} cm^{-2} sr^{-1})					
σ(S1) – total	2.25±0.45	7.10±0.35	3.65±0.15	2.70±0.15	2.00±0.60
σ(S1) – UV[d]	2.2±0.5	2.3±0.7	3.65±0.2	1.0±0.5	<0.8
σ(H_2) – UV[d]	130±30	140±50	220±30	70±40	<47
σ(S1) – Shock[d]	<0.4	4.7±0.7	<0.1	1.7±0.5	1–2
Cloud parameters					
n_H (cm^{-3})[d]	3000	5000	10 000	5000	2000:
[e]	3000	15 000	10 000	13 500	5000:
$L(H_2)$ ($L_\odot$)[d,f]	120±30	200±65	155±20	65±30	40?
[e,f]	120±30	600±120	155±20	175±30	130±40
$10^4\ L(H_2)/L_*$[d,f]	2.0±0.5	2.0±0.7	3.1±0.4	0.5±0.3	0.8?
[e,f]	2.0±0.5	6.0±1.4	3.1±0.4	1.4±0.3	2.6±0.8
$\sigma_{shock}(S1)/n_H$[d,f] (10^{-9} erg s^{-1} cm sr^{-1})	<1.3	9.4±1.4	<0.1	5.4±1.6	5–10

Notes
[a] Derived from (1–0 Q(3)/1–0 S(1)) ratio
[b] From optical data (see references in Sect. 3.1)
[c] $I_{UV}=1$ corresponds to I_{1000} Å$=4.5\ 10^{-8}$ photons s^{-1} cm^{-2} Hz^{-1} (cf. BvD)
[d] Assuming collisional de-excitation of fluorescent emission to be unimportant (see Sect. 3.3)
[e] Assuming no shock-excited emission to be present
[f] $L(H_2)$ not corrected for extinction, nor for extent

magnitude. If pressure equilibrium is required, one or more of the following conditions must be fulfilled: (a) the H_2 zone is clumped on scales of 0.1 pc or less; (b) the H_2 temperature is higher than 100 K, possibly as high as 1000 K; (c) where the H II region borders the H_2 zone, its density is only a few hundred H cm^{-3}. Note that (a) and (b) suggest the occurrence of collisional de-excitation, but that (c) cannot be ruled out. Again, we note that the densities in Table 4 are mean values assuming complete aperture filling. They are lower limits to the actual density.

3.5. Physical condition of shock-excited H_2

In SMC-N88, LMC-N159A5 and N160A2, a shock-excited H_2 component may be present. In Table 4 aperture-averaged upper limits to the surface brightness of shocked 1–0 S(1) emission are listed. As in all cases UV excitation dominates over shock excitation, the condition $n_H V_s^3 < 10^8$ (cm^{-1} km s^{-1})^3 should be fulfilled (Shull & Hollenbach 1978, Eq. B12). The lower limits to n_H in Table 4 do not significantly constrain shock velocities which are in the range $V_s < 22$ km s^{-1} for N83B and < 37 km s^{-1} for N160A2. If typically 10% of the aperture is filled, densities are raised tenfold, and the upper limits drop by a factor of two.

The densities n_H derived for the radiatively excited H_2 component scale with surface brightness $\sigma_{UV}(S1)$ and thus with aperture-filling factor. Assuming equal filling factors for UV and (possible) shock-excited H_2 emission, the ratio $\sigma_{shock}(S1)/n_H$ is independent of the actual aperture-filling factor. This ratio is included in Table 4; all objects have $\sigma_{shock}(S1)/n_H < 10^{-8}$, with particularly stringent limits for N81 and N88. This appears to rule out J-type shocks faster than $V_s = 10$ km s^{-1} (cf. Shull & Hollenbach 1979). In turn, this allows us to derive upper limits to the mechanical luminosity L_w of stellar winds emanating from the exciting stars in the observed objects. With $V_s < 10$ km s^{-1} and the H II region radii given in Table 4, the model by Castor et al. (1975) yields upper limits ranging between $L_w < 0.3\ 10^{32}\ n_H$ erg s^{-1} (N83B) and $L_w < 3.3\ 10^{32} n_H$ erg s^{-1} (N81). We find a ratio of wind luminosity to stellar luminosity $L_w/L_* < 2\ 10^{-8} n_H$ for N88, N83B and N159A52, and $< 1.4\ 10^{-7} n_H$ for N81 and N160A2. The limits for C-type shock are less stringent: using the calculations by Draine et al. (1983) we find upper limits to the shock velocity to range from $V_s < 23$ km s^{-1} (N88, N160A2) to $V_s < 15$ km s^{-1} (N83B), so that L_w/L_* becomes $< 7\ 10^{-7} n_H$ (N81, N160A2), $< 1\ 10^{-7} n_H$ (N88, N159A5) and $< 4\ 10^{-8} n_H$ (N83B). We emphasize that these are true upper limits: in N81 and N83B

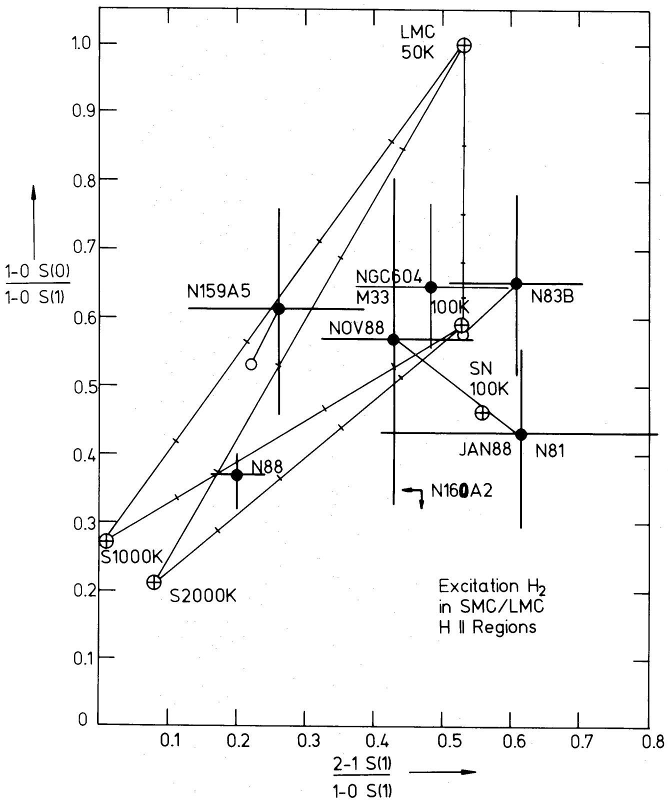

Fig. 4. Diagnostic line ratios of observed LMC/SMC sources and M33-NGC 604 (filled circles). Open circles denote dereddened ratios. Model ratios for radiatively excited H_2 gas under LMC ($T=50-100$ K; tick marks in steps of 10 K) and Solar Neighbourhood conditions ($T=100$ K) are also marked, as are model ratios for shock-excited H_2 gas (LTE emission at $T=1000$ and 2000 K). Ticks on the lines connecting radiative and shocked model ratios mark increasing radiative contributions to the 1–0 S(1) emission in steps of 20%

we have no actual indication for the presence of shock-excited emission, and in the other objects "thermal" fluorescent emission may have been mistaken for shock-excited emission.

Galactic O-stars of comparable stellar luminosity typically have a ratio $L_w/L_* = 2.5\ 10^{-3}$. Thus, the exciting stars of the observed Magellanic H II regions have stellar winds significantly weaker than similar Galactic stars, unless $n_H > 5\ 10^4\ \mathrm{cm}^{-3}$; only for N81 and N160A2 is the limit less stringent with $n_H > 10^4\ \mathrm{cm}^{-3}$. However, especially at densities $n_H > 10^5\ \mathrm{cm}^{-3}$ the occurrence of "thermal" fluorescent emission becomes rapidly more probable, further tightening the limits on possible shock-excited contributions and by implication on wind luminosities as well.

3.6. *Helium lines*

An interesting result, first noted in Paper II, is the detection of the helium lines He I ($4^3S-3^3P_0$), He I ($4^1S-3^1P_0$) at 2.112 and 2.114 μ respectively. With the IRSPEC resolution, the two lines are well separated, but generally a good detection is only obtained of the He I ($4^3S-3^3P_0$) line as is the case in the Galactic planetary nebula NGC 7027 (Smith et al. 1981). Its strength is significant compared to that of the 1–0 S(1) H_2 line: it is much stronger than this line in N160A1 and N160A2, while the six remaining detections have $F(\mathrm{He\ I})/F(1\text{–}0\ \mathrm{S}(1)) = 0.50 \pm 0.14$ as in NGC 7027. CVF spectra generally do not have sufficient resolution to separate the He I and H_2 lines. Thus, our results show that 1–0 S(1) H_2 line strengths determined with low-spectral resolution (CVF) detectors may be *significantly overestimated*. This has dire consequences for the interpretation of H_2 line ratios based on this transition: in the presence of a strong He I line at 2.112/2.114 μ, radiatively excited H_2 may be falsely classified as shock-excited H_2 in CVF spectra, especially if the signal-to-noise ratio of the 2–1 S(1) and 1–0 S(1) lines is low.

Storey (1982) derived a ratio $I(2.112)/I(2.114) = 3.3$ for the He I lines for $T_e = 10^4$ K; with the exception of N88, our results are compatible with this ratio. In Paper II, we gave 2.058 μ He I (2^1P-2^1S) line strengths for N81, N88, N11A and N159A5. In these objects the ratio $I(2.112)/I(2.058)$ is 0.070 ± 0.015, about a factor of three higher than estimated by Storey (1982). If higher electron temperatures and self-absorption in the 2^3S state apply, the discrepancy may be decreased to a factor of about 1.5 (cf. Robbins 1968a, b). On the other hand, the CVF aperture was about twice the IRSPEC aperture. If the He I emission fills the larger aperture, the line ratio becomes $I(2.112)/I(2.058) = 0.15 \pm 0.03$, more than doubling the discrepancy noted above. Similarly, our Brackett-γ data (Paper II) yield a ratio $I(2.112 + 2.114)/I(\mathrm{Br}-\gamma) = 0.038 \pm 0.007$ (0.084 ± 0.014 with aperture correction) which should be compared to a ratio $I(2.1)/I(\mathrm{Br}-\gamma) = 0.29\ \mathrm{He}^+/\mathrm{H}^+$ for $T_e = 10^4$ K given by Storey (1982). In Paper II, we noted that the observed ratio $I(2.058)/I(\mathrm{Br}-\gamma)$ is lower than expected, which we there ascribed to aperture-filling effects. Now it appears that the 2.112 and 2.114 μ He I lines are *stronger* than expected, whereas the 2.058 μ He I line is weaker than expected. Further investigation of this result might be worthwhile.

4. Conclusions

We summarize our principal results below:

(1) We have confirmed our previous detections of molecular hydrogen in five small Magellanic Cloud H II regions, and added three more. In addition, H_2 was rather marginally detected towards two other objects (LMC-N55 and N159S).

(2) The observed extent of the H_2 cloud towards SMC-N88 shows that it probably represents the warm interface between the small H II region and the larger and colder associated molecular cloud.

(3) Diagnostic H_2 line ratios obtained for five molecular hydrogen clouds show that energetically, radiative excitation is the dominant mechanism. Cloud temperatures are of the order of 100 K, although at least one cloud (N159A5) appears to be cooler with $T=50$ K. Aperture-averaged hydrogen densities range from $n_H = 2\ 10^3\ \mathrm{cm}^{-3}$ to $n_H = 10^4\ \mathrm{cm}^{-3}$, with a mean of $5\ 10^3\ \mathrm{cm}^{-3}$.

(4) The 1–0 S(1) emission of three of the clouds studied (N88, N159A5 and N160A2) may also contain a shock-excited contribution. Alternatively, in these clouds densities may be high enough for collisional de-excitation to at least partly thermalize the observed lower levels, thus mimicking shock-excited emission. In any case, the luminosity of shock-excited H_2 is in all objects significantly less than that of radiatively excited H_2.

(5) If J-type shocks are present, they will have velocities $V_s < 10\ \mathrm{km\ s}^{-1}$; for C-type shocks $V_s < 15-23\ \mathrm{km\ s}^{-1}$. The early-type stars embedded in the observed objects appear to have stellar wind luminosities lower than those of similar Galactic O-stars.

(6) The He I (4^3S–3^3P^0) and (4^1S–3^1P^0) lines in Magellanic Cloud H II regions appear to be stronger than expected, whereas the He I (2^1P–2^1S) line appears to be weaker. In CVF observations, He I emission may seriously contaminate 1–0 S(1) H_2 fluxes.

References

Black J.H., van Dishoeck E.F., 1987, ApJ 322, 412 (BvD)

Burton M., Puxley P., 1990, in: The Interstellar Medium in Galaxies, Summaries of Contributed Papers, eds. D.J. Hollenbach, H.A. Thronson, NASA CP 3084, p. 238

Castor J., McCray R., Weaver R., 1975, ApJ 200, L107

Draine B.T., Roberge W.G., Dalgarno A., 1983, ApJ 264, 485

Heydari-Malayeri M., Testor G., 1985, A&A 144, 98

Heydari-Malayeri M., Testor G., 1986, A&A 162, 180

Heydari-Malayeri M., Le Bertre T., Magain P., 1986, A&A 195, 230

Heydari-Malayeri M., Van Drom E., Leisy P., 1990, A&A 240, 481

Israel F.P., Koornneef J., 1988, A&A 190, 21 (Paper II)

Koornneef J., 1983a, A&AS 51, 489

Koornneef J., 1983b, A&A 128, 84

Koornneef J., Israel F.P., 1985, ApJ 291, 156 (Paper I)

Moorwood A., Biereichel P., Finger G., Lizon J.-L., Meyer M., Nees W., Paurean J., 1986, ESO Messenger 44, 19

Panagia N., 1973, AJ 78, 929

Robbins R.R., 1968a, ApJ 151, 497

Robbins R.R., 1968b, ApJ 151, 511

Shull J.M., Hollenbach D.J., 1978, ApJ 220, 525

Smith H.A., Larson H.P., Fink U., 1981, ApJ 244, 835

Stenrnberg A., Dalgarno A., 1989, ApJ 338, 197

Storey J.W.V., 1982, MNRAS 202, 105

Testor G., Pakull M., 1985, A&A 145, 170

Testor G., Lortet M.-C., 1987, A&A 178, 25